XI International Conference on Computational Plasticity. Fundamentals and Applications
COMPLAS XI
E. Oñate, D.R.J. Owen, D. Peric and B. Suárez (Eds)

MICROMECHANICAL ANALYSIS OF DAMAGE AND FRACTURE IN SANDSTONE ROCK SPECIMENS, USING ZERO-THICKNESS INTERFACE ELEMENTS

D. GAROLERA, I. CAROL AND C.M. LÓPEZ

Dept. of Geotechnical Engineering and Geo-Sciences
Universitat Politècnica de Catalunya. BarcelonaTech (UPC)
Campus Nord UPC, 08034 Barcelona, Spain
e-mail: daniel.garolera@upc.edu, Ignacio.carol@upc.edu

Key words: Rock mechanics, fracture, zero-thickness interface.

Abstract. This numerical study deals with the analysis of rock specimens from a micro-mechanical point of view. The analysis is based on the Finite Element Method (FEM) with fracture-based zero-thickness interface elements, and numerically generated micromechanical geometries. In previous studies this approach has been used very successfully to represent the mechanical behaviour of concrete and other quasi-brittle materials under a variety of loading scenarios. The current study, motivated by longer-term research on rock sanding in oil wells, is focused on the capability of the model to represent the type of failure observed near the walls of tunnels or holes bored in a medium subject to initial compressive stresses. In this context, the microstructure of sandstone rock is generated *via* Voronoi tessellation. Interface elements are inserted along all polygon contacts, and, for some calculations also within the polygons themselves. The two main loading scenarios explored are direct uniaxial compression, and uniaxial extension after hydrostatic loading. Besides a general good capability to represent the desired behaviour, the results show that direct uniaxial compression requires intra-granular cracks in the model in order to reach failure. However, if the same final loading state is reached via initial hydrostatic loading followed by uniaxial extension, (as typical in tunnel or borehole walls), then failure kinematics changes and failure may take place with the inter-granular interfaces exclusively (i.e. no need to consider intra-granular cracks to represent failure).

1 INTRODUCTION

In this paper, a micromechanical approach based on FEM with zero-thickness interface elements is described for the analysis of cemented granular materials such as sandstone rock, including the effects of inter-granular and intra-granular cracking and fracture. Instead of the phenomenological parameters used in the traditional continuum-based formulation of the FEM, the proposed methodology is capable of reproducing complex behaviour using only a few physical parameters, although this is at the expense of discretizing the grain microstructure explicitly. In previous studies this approach has been used very successfully to represent the mechanical behaviour of concrete and other quasi-brittle materials under a

variety of loading scenarios ([1], [2] and [3]).

2 MICROSTRUCTURAL MODELLING

2.1 Microstructure

In the current study, individual grains of the sandstone rock material are represented explicitly in the FE mesh. The geometry of the grains is generated numerically *via* Voronoi tessellation over a grid of points, which are randomly perturbed from their original regularly-spaced positions. Zero-thickness fracture-based interface elements [4] inserted between adjacent grains represent the behaviour of the inter-granular contact including the cementing material. With regard to the grains themselves, two different options have been explored: (1) the grains are considered as linear elastic and therefore they cannot crack, only inter-granular cracks are allowed in this first option; and (2) additional interface elements are inserted within each grain, along all radial lines connecting each grain corner to its center, so that intra-granular cracking becomes also possible (Fig.1).

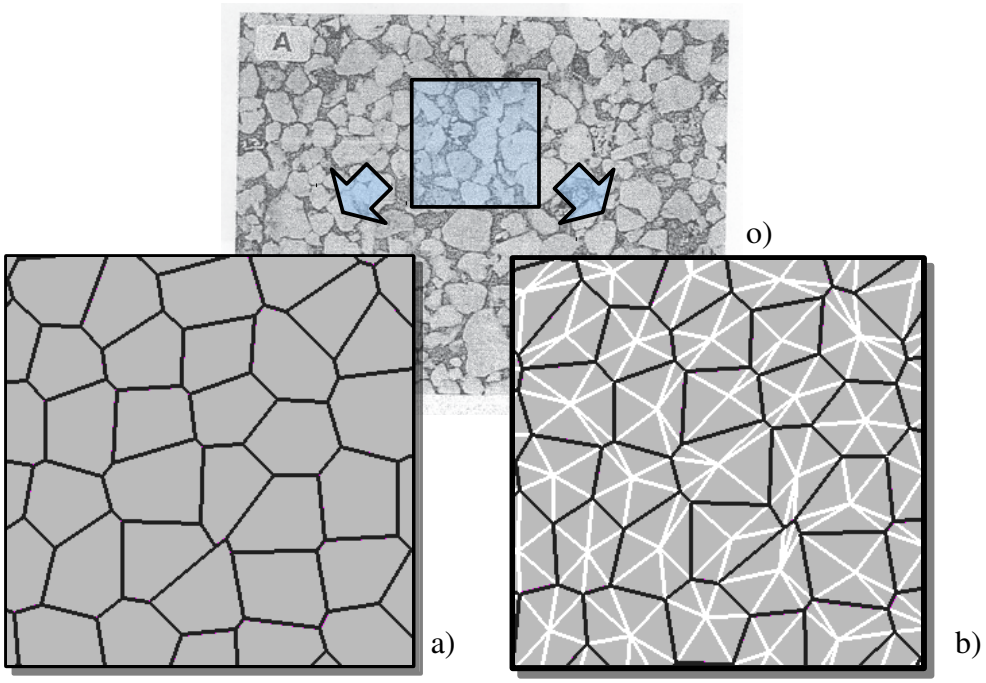

Figure 1: Microstructure representation. o) Micro-photograph from a sandstone sample; a) interface layout considering linear elastic grains (dark lines); and b) interface layout considering also the possibility of intra-granular cracks (pale lines).

2.2 Interface constitutive law

An essential ingredient of the approach described is the constitutive equation of the interface elements, which must be formulated in terms of normal and shear stress tractions (σ,τ) and the corresponding relative displacements (u,v). It consists of an elasto-plastic formulation incorporating some concepts of fracture mechanics. The model is defined by a hyperbolic fracture surface (yield surface) described by three parameters: c (cohesion),

χ (tensile strength) and ϕ (friction angle) (Eq. 1).

$$F\left(\sigma,p\left(W^{cr}\right)\right)=\tau^2-\left(c-\sigma\tan\phi\right)^2-\left(c-\chi\tan\phi\right)^2 \tag{1}$$

The evolution of the model parameters is controlled by an energy-based history variable W^{cr} (energy spent in fracture processes per unit area of the interface), the increments of which are calculated for each increment of the loading process using different expressions in tension and compression (case in which basic friction is substracted) (eq. 2):

$$dW^{cr}=\sigma\delta u_N^{cr}+\tau\delta u_T^{cr}\quad\left(\sigma\geq 0\right) \tag{2}$$

$$dW^{cr}=\tau\delta u_T^{cr}+\left(1-\left|\sigma\tan\phi/\tau\right|\right)\quad\left(\sigma<0\right)$$

The hardening/softening laws then define the evolution of the surface parameters in terms of the history variable W^{cr}, incorporating as parameters G_f^I (fracture energy in mode I) and G_f^{IIa} (fracture energy in mode IIa) [4].

The numerical integration of the constitutive law is implemented using an algorithm based on an implicit procedure (backward-Euler) with sub-incrementation [5]. One of the features of this procedure is that it provides an always consistent tangent matrix, even in the case of sub-increments.

3 RESULTS FOR THE HOLLOW CYLINDER TEST UNDER EXTERNAL PRESSURE

The study of this test is motivated by long-term research on sand production in oil wells [6]. In that context, the hollow cylinder test under increasing external pressure is widely used to understand wellbore stability problems. [7] and [8].

For simplicity, the numerical model was reduced to the analysis of a 2D transversal cross-section of the cylinder, under the assumptions of small deformation and plane strain (Figure 2). The darker inner corona of the domain was discretized using Voronoi polygons and interfaces, and the external pressure was applied on the outer boundary, while the prescribed nodes are reduced to a minimum of four (see Fig 2) in order to not to restrain the corresponding deformation. Given the material non-linearity provided by the interface elements, the external pressure was applied in small increments.

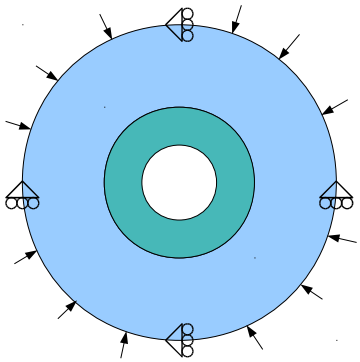

Figure 2: Schematic hollow cylinder test section with boundary conditions.

Some preliminary analyses of this case led to unexpected results. Using a friction angle of 30 degrees for the interfaces, under the level of expected failure pressure, the calculation was practically in elastic regime with hardly a few interfaces opening near the inner boundary. In order to get a failure pattern similar to experiments with the same mesh, the friction angle of the interfaces had to be lowered to unphysical values near 5 degrees.

A couple of images of the opened cracks and deformed mesh of the numerical solution in this case are shown in figure3. As it can be seen in the figure, in spite of the unrealistic friction value, the main failure patterns reported in the experimentation literature [7] are well captured: spalling (tensile break-offs) and shear-bands (breaks in shear compression mode that produce some typical spirals).

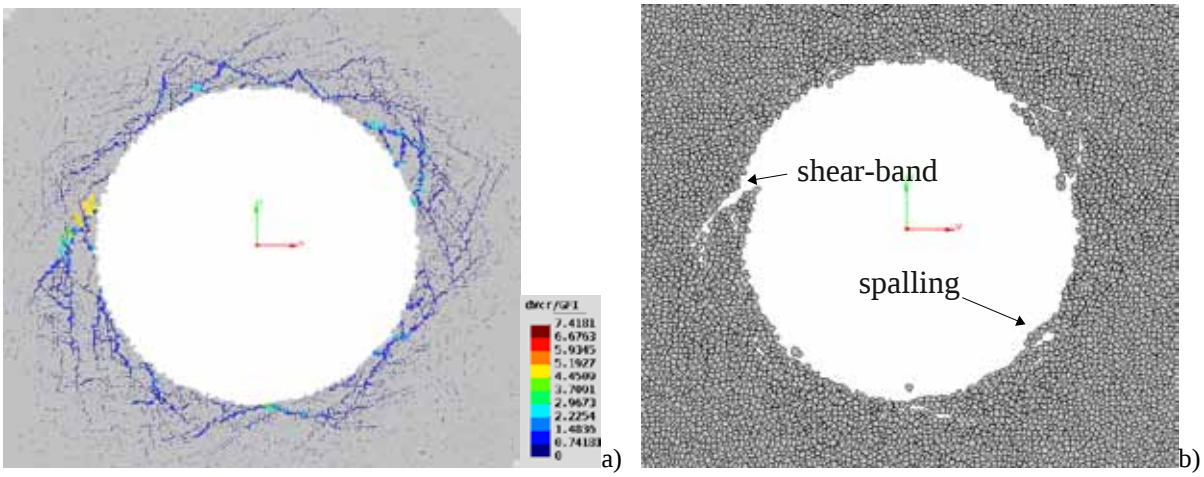

Figure 3: numerical results for tan(5); left, energy spent of fracture at the end of the load application; right, final deformation mesh (x25).

However, unrealistic friction angles were considered unacceptable and attention was turned onto a different option: introducing interface elements across grains, in order to allow for the development of intra-granular cracks. However, introducing intra-granular interface elements in the previous FE mesh, in the way shown in figure 1b, increases considerably the number of degrees of freedom. For this reason the study of this new approach to the problem was first studied on smaller specimens.

4 UNIAXIAL COMPRESSION AND EXTENSION TESTS OF 1X1CM SPECIMENS

The specimens considered for introducing inter-granular interfaces are square specimens with dimensions 1x1cm^2 and grain size of about 0,25 mm, which leads to approximately 40x40 grains over the specimen as represented in figure 4a. In order to open the possibility of intra-granular cracking, zero-thickness interface elements have been inserted, not only along the inter-granular boundaries, but also across grains, as depicted in figure 1b. This specimen has been analysed under uniaxial compression, and under hydrostatic pressured followed by uniaxial extension scenarios.

In order to evaluate the influence of intra-granular cracking, three different assumptions

have been considered regarding the strength parameters of intra-granular interfaces:

a. They are assumed as linear-elastic (and very high stiffness K_N and K_T); in this case these interfaces, even if present, cannot crack.
b. They are allowed to crack, but strength parameters have double values than those of inter-granular interfaces.
c. They are allowed to crack, with same strength parameters as inter-granular interfaces.

Table 1 contains the list of parameters used in the calculations.

Table 1: Material properties used in simulations.

Grain (cont.)	**Inter-grain interface**	**Intra-grain interface**	
		Fracture-grain	**Fracture-grain (double)**
E = 34.0e3 MPa	Kn = 1.0Ee9 MPa/m	Kn = 1.0Ee9 MPa/m	Kn = 1.0Ee9 MPa/m
ν = 0.27	Kt = 1.0Ee9 MPa/m	Kt = 1.0Ee9 MPa/m	Kt = 1.0Ee9 MPa/m
	Tan(ϕ) = 0.5773	Tan(ϕ) = 0.5773	Tan(ϕ) = 0.8389
	χ = 1.0 MPa	χ = 1.0 MPa	χ = 2.0 MPa
	C = 4.0 MPa	C = 4.0 MPa	C = 8.0 MPa
	GfI = 1.0E-5 MPa*m	GfI = 1.0E-5 MPa*m	GfI = 2.0E-5 MPa*m
	GfI = 1.0E-4 MPa*m	GfI = 1.0E-4 MPa*m	GfI = 2.0E-4 MPa*m
	σ_{dil} = 10.0 MPa	σ_{dil} = 10.0 MPa	σ_{dil} = 20.0 MPa

4.1 Uniaxial compression test

Figure 4 depicts the geometry of the mesh and the boundary conditions used in this case. Load application is performed by means of a prescribed displacement on the upper side of the specimen. Due to the expected softening behaviour, an arc-length strategy was employed to control post-peak response.

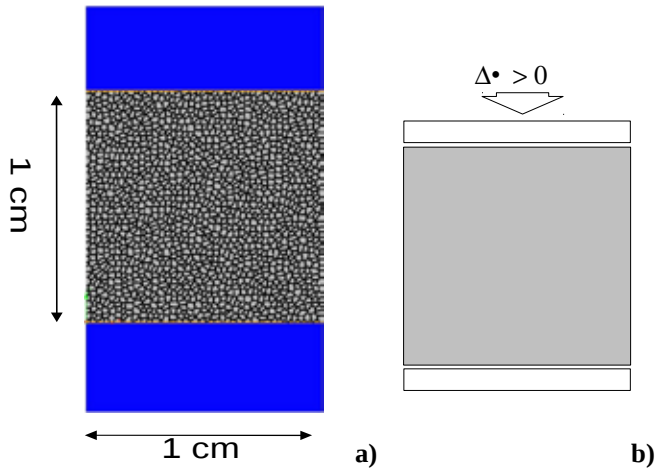

Figure 4: Uniaxial compression test. a) geometry; b) boundary conditions.

Figure 5 shows the average strain-stress curves obtained for the three scenarios of intra-

granular strength. It can be observed that intra-granular strength values influence dramatically the resulting behaviour of the overall material. Not allowing intra-granular cracking leads to an upper bound of the mechanical behaviour for which failure under uniaxial compression is never reached. On the other end, case c) approaches the behaviour of a quasi-brittle material without the granular structure considered (since cracks can develop equally through grains as in between grains), which leads to a lower bound of the overall strength; and finally option b) with the right parameters should represent a more realistic intermediate case.

As it can be also seen in Fig 5, the material post-peak response is also greatly influenced by grain resistance; as intra-grain resistance is increased, the model behaviour becomes more brittle.

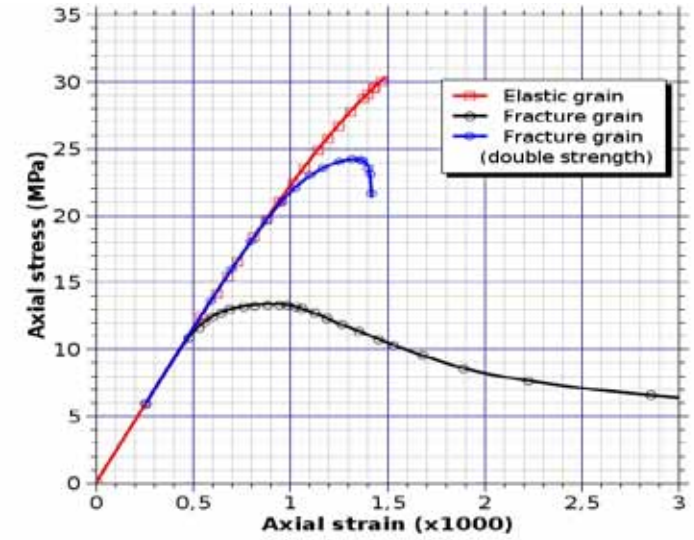

Figure 5: Average strain-stress curves for the uniaxial compression simulations, with the three different assumptions for intra-granular cracking.

In figure 6, the general crack pattern obtained and some enlarged detail of a section of a main macro-crack, are depicted for the three assumptions of intra-granular strength. For case b) with double strength, it may be clearly observed that cracks are basically opening/sliding around grains except at certain very specific points where grains crack due to the high stress concentration, while for case c) this happens systematically, and for case a) this does not happen at all. These details of micromechanical cracking may help understanding the resulting overall stress-strain curves of figure6. A first conclusion of these results is that the direct uniaxial compression test is very sensitive to grain strength, and that some form of intra-granular cracking must be allowed for a realistic description of the direct uniaxial compression test of a granular material using Voronoi-generated grain geometry.

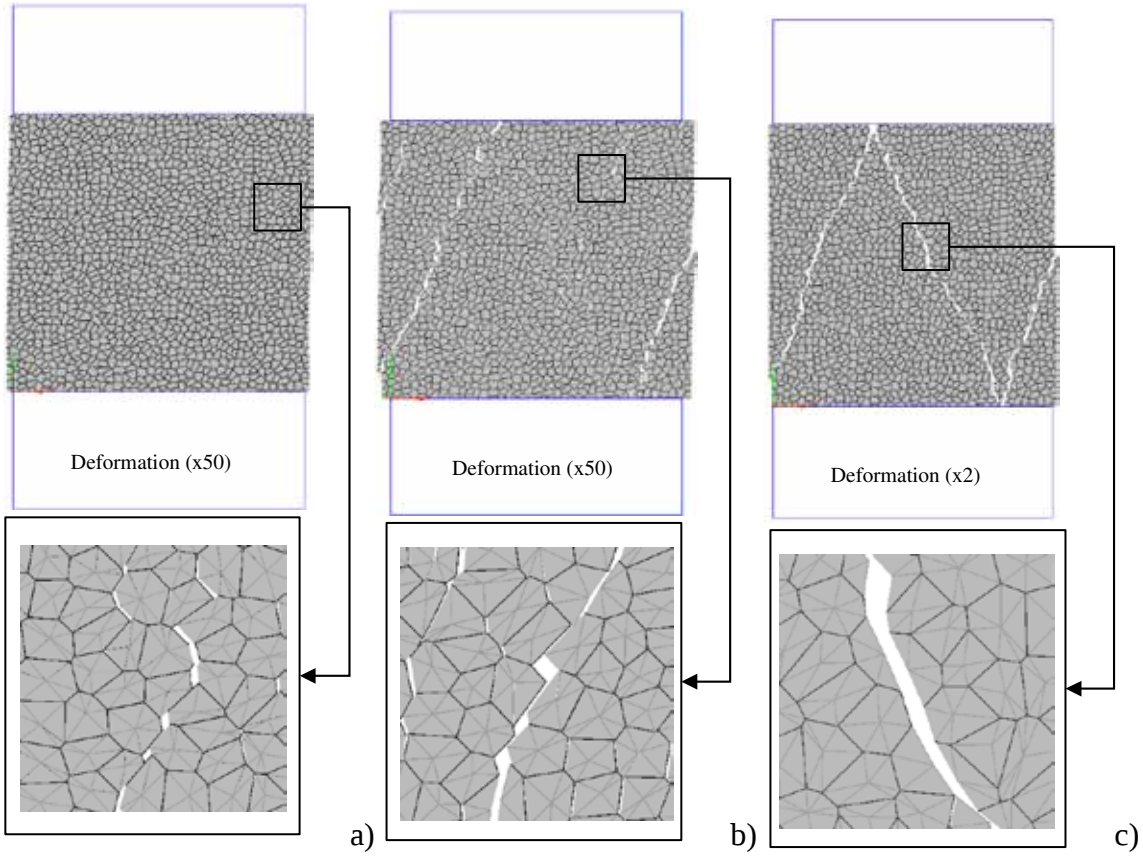

Figure 6: Mesh deformations for UCT at different values of grain resistance: a) elastic grains; b) fracture grains (double resistance) and c) fracture grains (single resistance).

4.2 Uniaxial extension test

The micro-structural grain geometry and meshes for this analysis are the same used for the uniaxial compression test in the precedent Sect 4.1. The first set of calculations is obtained without allowing intra-granular cracks, i.e. the grains are considered linear elastic. The loading and boundary conditions are represented in figure 7, and are applied in two steps: first, a hydrostatic stress is applied as a distributed load over top and right sides of specimen, while left and lower sides sit on rigid frictionless platens. And second, a progressively increasing horizontal displacement (extension) is prescribed to the right platen, while load is maintained constant in the vertical direction. In this way, the horizontal stress will be progressively decreased, therefore in the limit approaching a uniaxial compression. Note that this is the same final state as applied in the previous section, although in this case this is achieved following a totally different stress path, and that will make a significant difference.

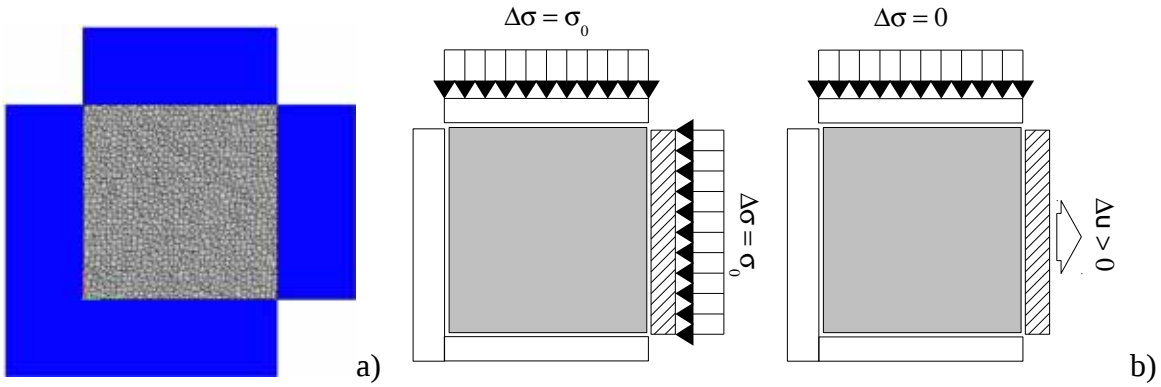

Figure 7: Extension test. a) geometry; b) boundary conditions.

This analysis (with elastic grains) has been repeated for different values of the initial hydrostatic load, and the results obtained are shown in figures 8 and 9. In figure 8, the average stress-strain curves for the specimen are represented, with the (computed) horizontal average stress on the vertical axis, and the corresponding average strains on the left horizontal axis. On the right horizontal axis, the transversal (in this case vertical) average strain is represented. Note that in this direction load is maintained constant. In the curves it is shown that as the initial confinement is higher, the material behaviour becomes more ductile, with a progressively more reduced tensile response, which, eventually (for a sufficiently high initial confinement) disappears altogether.

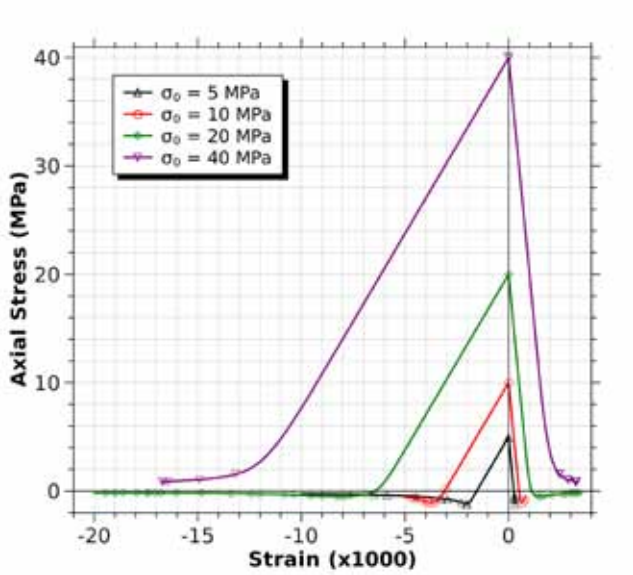

Figure 8: Strain-stress relationship for the extension test. The graph shows, for the intra-grain elastic case, results at different confinement levels.

In figure 9, the horizontal displacement field obtained at the end of the same calculations is shown via deformed meshes with a superimposed gray scale. The diagrams clearly show that the lower the initial confinement stress, the more brittle failure becomes. Likewise, the lower

the initial confinement, the more pronounced the cracking is, and the more clearly localized into macro-cracks the displacement jumps become, in contrast to the almost uniformly distributed cracking observed for the case of highest confinement σ = 40 MPa (lower right diagram).

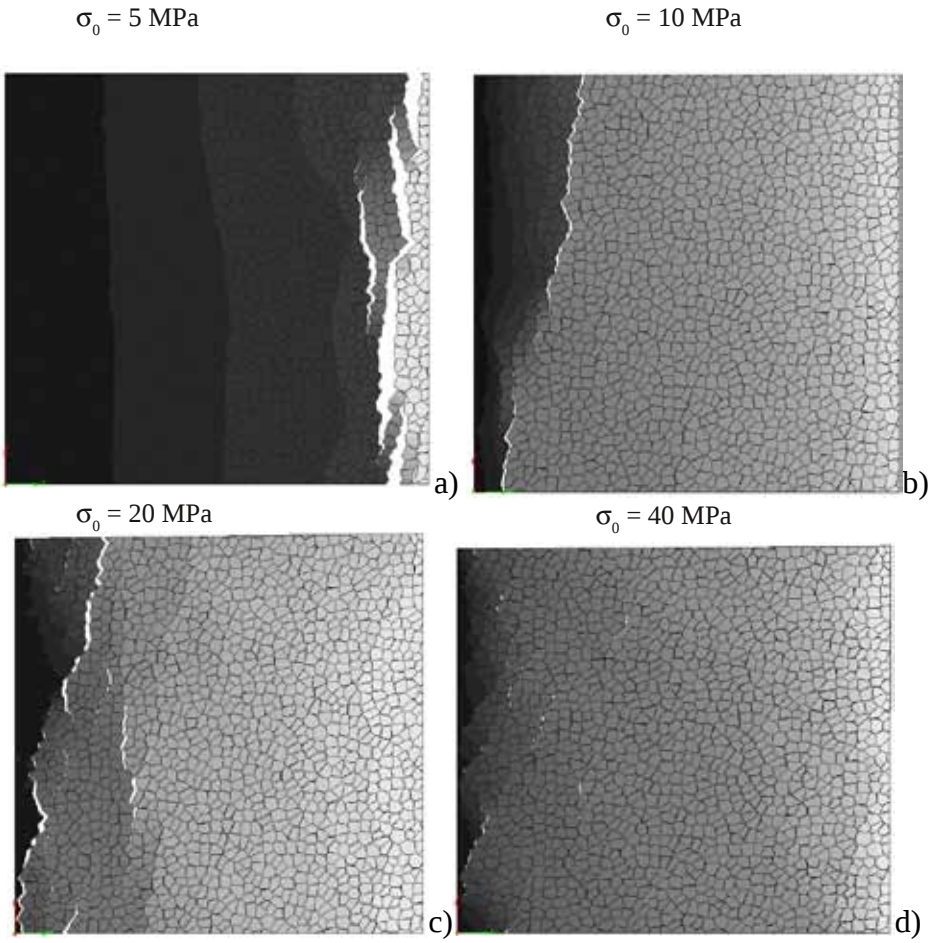

Figure 9: Deformation meshes (x5) for extension test for different initial confining pressures with elastic grains. a) σ_0 = 5 MPa; b) σ_0 = 10 MPa; c) σ_0 = 20 MPa and d) σ_0 = 40 MPa.

The effect of intra-granular cracking is also studied for this uniaxial extension test, by carrying out two additional calculations in which intra-granular interfaces are allowed to crack, one of them with same strength parameters as the inter-granular cracks, and the other with roughly double strength (same sets of parameters already used for the uniaxial compression test, see Table 1). Both calculations were performed for the same initial confinement pressure of 10 MPa, and the results can be compared to the results for this level of initial confinement and elastic grains already shown in previous figures 8 and 9.

In figure 10, the average stress-strain curves along the horizontal direction are represented for the two new cases with intra-granular cracking, together with the previous curve of elastic grains. In figure 11 the fields of horizontal deformation obtained in these calculations are depicted. It can be seen that the curves for elastic grains and for fracturing grains with higher

strength (that, from the material perspective, is a definitely more realistic assumption than that of equal strength) look very much alike. This, on the other hand, seems consistent with a kinematics of extension, cracks being opened predominantly in tensile mode I rather than the shear mode observed in the direct compression test (Sec. 4.1).

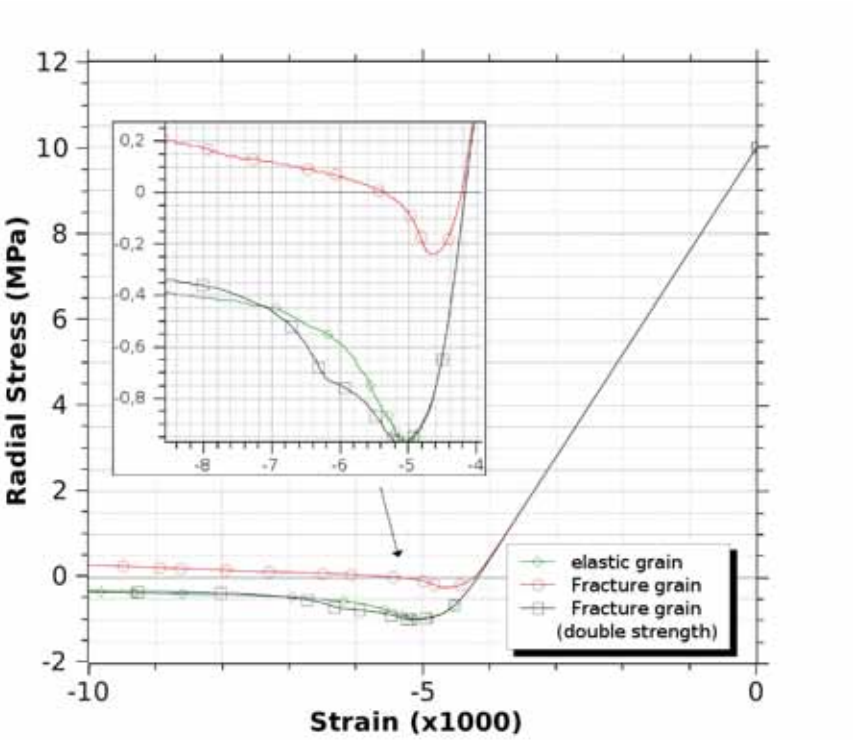

Figure 10: Average strain-stress curves for the extension test, assuming: a) elastic grains; b) fracturing grains (double strength) and c) fracturing grains (same parameters as inter-granular cracks).

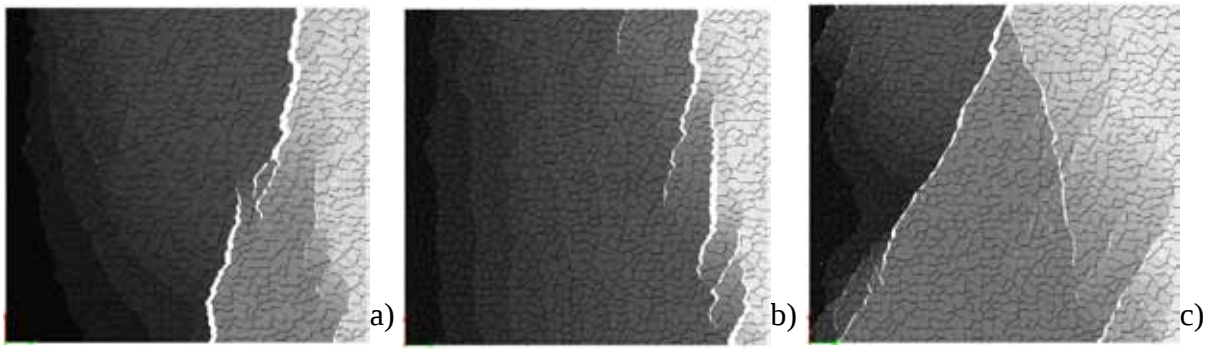

Figure 11: Horizontal deformation field for the uniaxial extension test for 10 MPa of initial confining pressure, assuming: a) elastic grains; b) fracturing grains (double strength) and c) fracturing grains (same parameters as inter-granular cracks).

5 CONCLUSIONS REMARKS

Micromechanical analysis via FEM with zero-thickness interface elements and Voronoi-

generated geometries seems capable of reproducing fracture propagation in cemented granular rock materials. In particular, the results presented show that, for direct uniaxial compression, intra-granular failure must be considered in the analysis in order to capture the overall failure kinematics and realistic peak loads. However, if the same uniaxial compressive stress failure state is reached via a more complex loading paths such as uniaxial extension in the transverse direction after an initial hydrostatic state, the kinematics of failure changes significantly from sliding to opening, and similar meshes without intra-granular interfaces seem sufficient to realistically represent failure.

4 ACKNOWLEDGEMENTS

This research is supported by grant BIA2009-10491, funded by MICINN (Madrid, Spain). The first author also wishes to acknowledge his current support from project 2009SGR-180 funded by AGAUR-Generalitat de Catalunya (Barcelona).

REFERENCES

[1] Carol, I., López, C. M. and Roa, O., "Micromechanical analysis of quasi-brittle materials using fracture-based interface elements". International Journal for Numerical Methods in Engineering, 52, p. 193-215 (2001).

[2] López, C. M., Carol I. and Aguado, A., "Meso-structural study of concrete fracture using interface elements. I: numerical model and tensile behavior". Materials and Structures, Vol. 41(3), p. 583-599 (2008).

[3] Caballero, A., Carol, I. and López, C. M., "A meso-level approach to the 3D numerical analysis of cracking and fracture of concrete materials". Fatigue and Fracture of Engineering Materials and Structures, Vol. 29(12), p. 979-991 (2006).

[4] Carol, I., Prat, P. and López, C.M., "A normal/shear cracking model. Application to discrete crack analysis" ASCE J. Engrg. Mech., Vol 123(8), p. 765-773 (1997).

[5] Caballero, A., Willam, K. and Carol, I., "Consistent tangent formulation for 3D interface modeling of cracking/fracture in quasi-brittle materials". Computer Methods In Applied Mechanics And Engineering, Vol. 197, p. 2804-2822 (2008).

[6] Garolera, D., López, C.M., Carol, I. and Papanastasiou, P., "Micromechanical analysis of the rock sanding problem". Journal of the Mechanical Behaviour of Materials. Vol. 16(1-2), p. 45-53. (2006).

[7] Cook, J.M., Bradford, I.D. and Plumb, R.A., "A study of the physical mechanisms of sanding and application to sand production prediction". Presented in European Petroleum Conference in London, UK, October 1994. SPE paper No. 28852, (1994).

[8] Papamichos, E., Tronvoll, J., Vardoulakis, I., Labuz, J.F., Skjærstein, A., Unander, T.-E. and Sulem, J., "Constitutive testing of Red Wildmoor sandstone". Mech. Cohes.-Frict. Mater. 5(1), p. 1-40 (2000).